Spin-valley resolved photon-assisted tunneling in carbon nanotube double quantum dots

E. N. Osika and B. Szafran

AGH University of Science and Technology, Faculty of Physics and Applied Computer Science, al. Mickiewicza 30, 30-059 Kraków, Poland

(Received 1 March 2017; published 12 May 2017)

We consider photon-assisted tunneling (PAT) and the Landau–Zener–Stueckelberg (LZS) interference for double quantum dots induced electrostatically along a semiconducting carbon nanotube. An atomistic tight-binding approach and the time-dependent configuration-interaction method are employed to describe systems of a few confined electrons and holes. We reproduce the patterns of the LZS interference recently observed for quantum double dots describing transport across hole-localized states. Moreover, we indicate that for charge configurations for which the ground state is Pauli-blocked, PAT can be used for resolution of the transitions that involve spin-flip or intervalley transitions without the spin-valley conserving background signal.

DOI: 10.1103/PhysRevB.95.205305

I. INTRODUCTION

Photon assisted tunneling (PAT) across quantum dots (QDs) [1–3] is observed in microwave fields when the Fermi-level electrons pass across the higher-energy confined levels upon absorption of the energy from the radiation field. The phenomenon has a resonant character and occurs provided that the microwave frequency is in resonance with the mismatch between the energy levels ΔE so that the electron absorbs a single or n photons in order to climb to the higher energy level, $n\hbar\omega = \Delta E$. PAT has been used for spectroscopy of dot-confined energy levels [3–5] and charge dynamics in multiple quantum dots [6–8]. PAT in double quantum dots has also been used for spin-related phenomena including transport involving spin flips [9] and manipulation of spin qubits [10,11]. For strong microwave fields within double quantum dots the PAT enters the regime of the Landau–Zener–Stueckelberg (LZS) [12,13] interference when the system is driven by an ac electric field across the avoided crossing between energy levels of different charge occupation. The procedures for fast spin flips based on the LZS interference were proposed [7,14,15]. The LZS interference pattern has also been used for studies of the dephasing processes [12,16] in double dots, including the spin coherence times [17–19], as well as for sensitive residual radiation detectors [20], charge [21,22], and spin pumping [23].

The PAT and LZS interference were also observed in quantum dots defined in semiconducting carbon nanotubes (CNTs) [5,16]. In CNTs—the graphene-related material with strong spin-orbit coupling due to the curvature of the carbon plane [24–29]—in addition to the spin degree of freedom the valley degree of freedom is present. In this paper we consider detection of photon-assisted tunneling involving spin flips and intervalley transitions. The study is based on the time-dependent configuration-interaction approach for systems of several carriers described within the atomistic tight-binding approach. The study covers simulation of the LZS interference pattern as recently observed [16]. Moreover, we indicate that, for systems in which the charge transport is blocked by the Pauli blockade, the LZS pattern contains clear separate lines corresponding to either the spin or valley flips accompanying the electron hopping.

II. THEORY

We model a semiconducting CNT of length $L = 53.11$ nm, diameter $2r = 1.33$ nm, and chiral vector $C_h = (17,0)$. We consider both a straight nanotube and a bent [30] one with radius of the bend $R = 40$ nm [see Fig. 1(a)]. The nanotube is suspended above the electrostatic gates which produce a double quantum dot confining potential

$$W_{\mathrm{QD}}(z) = V_1 e^{-(z+z_s)^2/d^2} + V_2 e^{-(z-z_s)^2/d^2}. \tag{1}$$

In Eq. (1) d determines the QD widths, z_s is a shift of the dots from $z = 0$, and V_1 (V_2) is a potential of the left (right) QD. We consider nanotube in pp and nn configurations in which both dots are occupied by either holes or excess electrons, respectively. For a pp configuration we apply $V_1 = V_p$, $V_2 = V_p - \Delta$, and for the nn configuration $V_1 = V_n - \Delta$, $V_2 = V_n + \Delta$, where Δ defines the energy mismatch between potentials on the left and right dot. In the calculations we apply $V_p = 0.3$ eV, $V_n = -0.5$ eV, $z_s = 10$ nm, and $d = 4$ nm. We apply an external magnetic field of magnitude B parallel to the z direction.

We calculate single-electron states in the tight-binding approximation with the p_z orbitals. The Hamiltonian reads

$$H = \sum_{\{i,j,\sigma,\sigma'\}} \left(c^\dagger_{i\sigma} t^{\sigma\sigma'}_{ij} c_{j\sigma'} + \mathrm{H.c.}\right) + \sum_{i,\sigma,\sigma'} c^\dagger_{i\sigma}\left(W_{\mathrm{QD}}(\mathbf{r}_i)\delta_{\sigma\sigma'} + \frac{g_L\mu_b}{2}\boldsymbol{\sigma}^{\sigma\sigma'}\cdot\mathbf{B}\right)c_{i\sigma'}. \tag{2}$$

The first sum in Eq. (2) accounts for the hopping between the nearest-neighbor atoms and the second sum for the interaction with the external electric and magnetic fields. Here $c^\dagger_{i\sigma}$ ($c_{i\sigma}$) is the particle creation (annihilation) operator at ion i with spin σ, $t^{\sigma\sigma'}_{ij}$ is the spin-dependent hopping parameter, $\delta_{\sigma\sigma'}$ stands for the Kronecker delta, $g_L = 2$ is the Landé factor, μ_b is the Bohr magneton, and $\boldsymbol{\sigma}$ is the vector of Pauli matrices. The hopping parameters $t^{\sigma\sigma'}_{ij}$ contain the spin-orbit interaction (SO), which arises from the curvature of the graphene plane [24–29]. Both the folding of the graphene plane into the tube and the bend of the nanotube [31] are taken into account. Moreover,

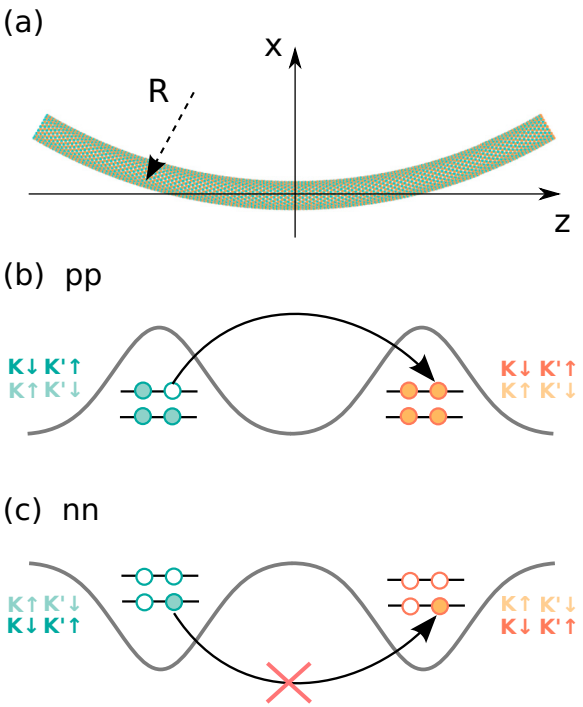

FIG. 1. (a) Scheme of the system considered in the paper. The CNT is either straight with the axis that coincides with the z axis, or bent within the xz plane for the radius of the arc $R = 40$ nm. (b) $(1h,0)$ and (c) $(1e,1e)$ charge configuration of the pp and nn quantum dots, respectively. The arrows indicate (b) the $(1h,0) \rightarrow (0,1h)$ and (c) the $(1e,1e) \rightarrow (0,2e)$ transitions.

$t_{ij}^{\sigma\sigma'}$ include the Peierls phase which accounts for the interaction of the orbital magnetic moments with the external magnetic field. The explicit form of the hopping parameters has been given in Ref. [31].

We calculate few-electron eigenstates by using the configuration-interaction (CI) method. We solve the eigenproblem of the Hamiltonian

$$H_{\rm CI} = \sum_a \epsilon_a g_a^\dagger g_a + \frac{1}{2}\sum_{abcd} V_{ab;cd} g_a^\dagger g_b^\dagger g_c g_d, \qquad (3)$$

where ϵ_a is the energy of the ath eigenstate of Hamiltonian H, $g_a^\dagger$ and g_a are the creation and annihilation operators of the electron in the ath state, and $V_{ab;cd}$ are electron-electron interaction matrix elements (with the form given in Ref. [32]).

For pp quantum dots we focus on a $(1h,0)$ charge configuration (a single hole localized in the left dot) and its transition to the $(0,1h)$ state (a single hole localized in the right dot). To model the system we consider the seven last electrons of the two highest valence-band orbitals [see Fig. 1(b)] confined in the left and right dot, each of the orbitals nearly fourfold degenerate with respect to the valley and the spin—i.e., the system with a single unoccupied state of the valence band. For nn quantum dots we study the charge configurations for which Pauli blockade appears, i.e., $(1e,1e)$ (one electron in each dot) and its transition to $(0,2e)$ (two electrons in the right dot). For that transition we consider two electrons at the bottom of the conduction band [see Fig. 1(c)] and include the eight lowest conduction-band orbitals (32 states) in the CI basis.

The dynamics of the system driven by an external ac field is simulated by solving the time-dependent Schrödinger equation. The time-dependent Hamiltonian reads

$$H'(t) = H_{\rm CI} + \sum_{j=1}^{N} eFz_j \sin(\omega t), \qquad (4)$$

where F is the ac electric-field amplitude, ω is its frequency, N is the number of electrons (seven for pp and two for nn quantum dots). We solve the time-dependent Schrödinger equation within the basis of the eigenstates Ψ_n of Hamiltonian $H_{\rm CI}$,

$$\Psi(\mathbf{r}_{1,\ldots,N},\boldsymbol{\sigma}_{1,\ldots,N},t) = \sum_n c_n(t)\Psi_n(\mathbf{r}_{1,\ldots,N},\boldsymbol{\sigma}_{1,\ldots,N})e^{-\frac{iE_nt}{\hbar}}. \qquad (5)$$

In this basis the Schrödinger equation $i\hbar\frac{\partial\Psi}{\partial t} = H'\Psi$ takes the form

$$i\hbar\dot{c}_k(t) = \sum_n c_n(t)eF\sin(\omega t)\langle\Psi_k|z|\Psi_n\rangle e^{-\frac{i(E_n-E_k)t}{\hbar}}. \qquad (6)$$

We discretize Eq. (6) in time by using the Crank–Nicolson algorithm.

III. RESULTS

A. Photon-assisted $(1h,0) \rightarrow (0,1h)$ transitions

In Fig. 2(a) we present the single-hole lowest-energy levels of pp system as a function of the potential difference Δ between the dots. For equal potentials on both dots ($\Delta = 0$) the hole in the lowest-energy states occupies both dots evenly. Note that the levels of the $(1h,0)$ and $(0,1h)$ branch are nondegenerate at $\Delta = 0$. The avoided crossing of width 0.249 meV due to the tunnel coupling between the dots will be used in simulation of the LZS interference. For positive Δ the

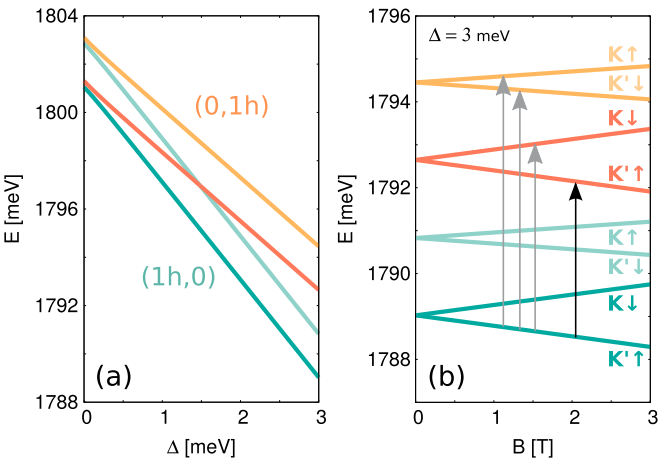

FIG. 2. (a) Single-hole energy levels in a pp QD as a function of the potential difference Δ between the dots for $B = 0$. (b) Energy-level dependence on the external magnetic field B for $\Delta = 3$ meV. The symbols $K/K' \uparrow / \downarrow$ indicate the spin-valley states of the hole [the single unoccupied energy level of the octet at the top of the valence band—cf. Fig. 1(b)] and the arrows represent possible $(1h,0) \rightarrow (0,1h)$ transitions.

$(1h,0)$ charge configuration is promoted to the ground state. Each line in Fig. 2(a) is twofold degenerate. The degeneracy is lifted by the external magnetic field B, as shown in Fig. 2(b). The symbols K/K', $\uparrow$ / $\downarrow$ indicate the valley and spin states of the hole (the only empty state in the valence band). The energy levels corresponding to the $(1h,0)$ and $(0,1h)$ charge configurations at $\Delta = 0$ in Fig. 2(a) are split by the spin-orbit interaction. The splitting between the orange and the blue lines in each of the configurations is of the order of 2 meV.

We focus on the transitions between $(1h,0)$ states (blue lines in Fig. 2) and $(0,1h)$ states (orange lines). These can be understood as the hole jumping from the left dot to the right one. We assume that the hole initially occupies the $K'\uparrow$ ground state. In straight, clean carbon nanotubes the hole can tunnel to the right dot only by the transition to the same spin and valley state [black arrow in Fig. 2(b)]. Transition to the states of different spin and/or valley [gray arrows in Fig. 2(b)] are possible provided that the symmetry of the nanotube is broken: the spin-orbit coupling itself does not allow for the spin transitions [33] and a short-range defect is needed to drive the valley flips [34]. Mixing of the spin or valley degree of freedom can be obtained by bending the nanotube or introducing disorder in the lattice, respectively.

In Fig. 3 we plot the probability of the transition $(1h,0) \rightarrow (0,1h)$ in a straight and clean CNT as a function of Δ and a logarithm of the amplitude of the microwave field F. The microwave frequency of $\hbar\omega = 0.5$ meV was assumed and the simulation time covered 1 ns. In Fig. 3 several transition lines can be observed which correspond to the direct transition from the $(1h,0)$ $K'\uparrow$ state to the $(0,1h)$ $K'\uparrow$ state (denoted as "1" in Fig. 3) and its harmonics ("1/2," "1/3," etc.) for multiphoton transitions [13]. The dashed line indicates the

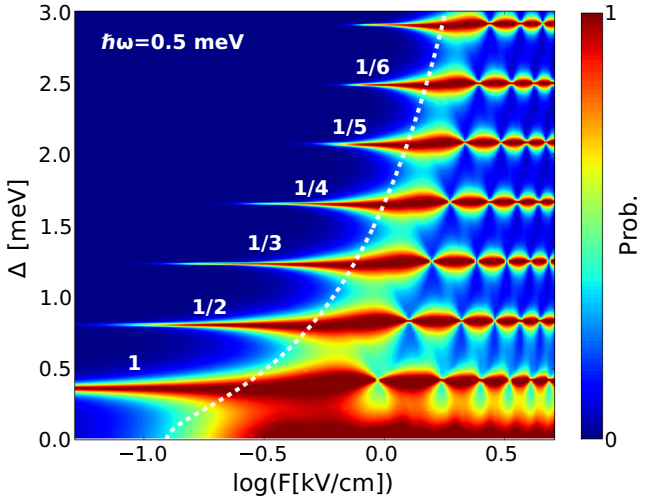

FIG. 3. Maximal probability of $(1h,0)K'\uparrow \rightarrow (0,1h)K'\uparrow$ transition for straight and clean CNTs as a function of Δ and a logarithm of the amplitude of the microwave electric field F. We apply the frequency $\hbar\omega = 0.5$ meV within a pulse of duration 1 ns. White numbers on the plot indicate the multiphoton resonances at 1, 1/2, 1/3, etc. of the nominal resonant frequency for the $(1h,0)K'\uparrow \rightarrow (0,1h)K'\uparrow$ transition. The thick dashed line shows the electric field required to take the system to the center of the avoided crossing between the $(1h,0)$ and $(0,1h)$ energy levels for a given detuning Δ.

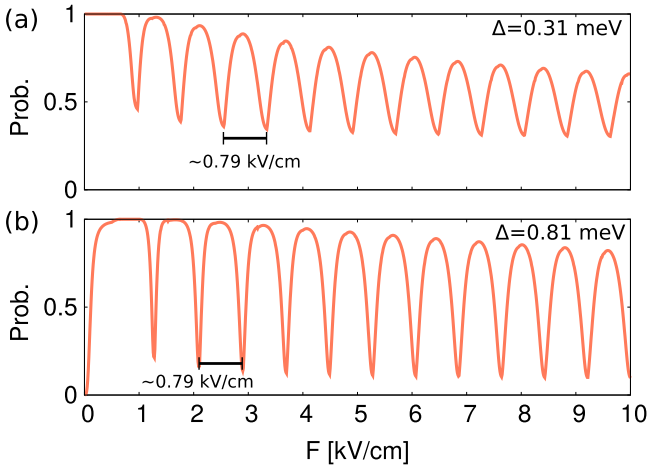

FIG. 4. Cross sections of Fig. 3—the maximal transition probability versus the ac electric field amplitude for (a) $\Delta = 0.31$ meV [direct $(1h,0)K'\uparrow \rightarrow (0,1h)K'\uparrow$ transition] and (b) $\Delta = 0.81$ meV (two-photon transition).

axial electric field that is necessary to reach the center of the avoided crossing of the $(1h,0)$, $(0,1h)$ configurations for a given Δ, i.e., $F = \frac{E_{(0,1h)}(\Delta) - E_{(1h,0)}(\Delta)}{2ez_s}$. To the right of the dashed line the electric field drives the system across the $(1h,0)$, $(0,1h)$ avoided crossing which allows for observation of the LZS interference. A clear interference pattern appears to the right of this line in Fig. 3. Together with the periodic variation of the electric field $eFz\sin(\omega t)$ the system goes back and forth across the $(1h,0) \leftrightarrow (0,1h)$ avoided crossing. Each passage through the avoided crossing region results both in a nonadiabatic transition between the states and in acquisition of the additional phases by them—different for $(1h,0)$ and $(0,1h)$ states. Depending on the relative phase acquired by the system during the time evolution we observe either constructive or destructive interference. It has been shown in Ref. [12] that, within the slow-passage limit, the position of the minima or maxima of the probability is proportional to the F/ω ratio. In Fig. 4 we plot the cross sections of Fig. 3 for $\Delta = 0.31$ meV [Fig. 4(a)] and $\Delta = 0.81$ meV [Fig. 4(b)] with the linear F scale. Both for direct [Fig. 4(a)] and two-photon [Fig. 4(b)] transitions we indeed observe equal distances of about 0.79 kV/cm on F scale between the consecutive extrema of the probability, which confirms the LZS origin of the observed oscillations. Since away from $\Delta = 0$ the energy levels depend linearly on Δ [see Fig. 2(a)], the distance between the adjacent harmonics on the Δ scale is constant. The results of Fig. 3 agree with those obtained in the experiment of Ref. [16].

In Fig. 5(a) we reproduce the results of Fig. 3 for a bent CNT. The bending mixes the spins and allows for the hole transition from one dot to the other accompanied by a spin flip. The lines appearing due to the bending correspond to the transition from $(1h,0)$ $K'\uparrow$ state to $(0,1h)$ $K'\downarrow$ state at one fifth, one sixth, and one seventh of the nominal resonant frequency. The distance between the harmonics on the Δ scale is constant since the energy difference between the two states participating in the transition is linear in Δ [see Fig. 2(a)]. Moreover, the Δ distances between adjacent harmonics are the same for spin-conserving and spin-flipping transitions. However, the

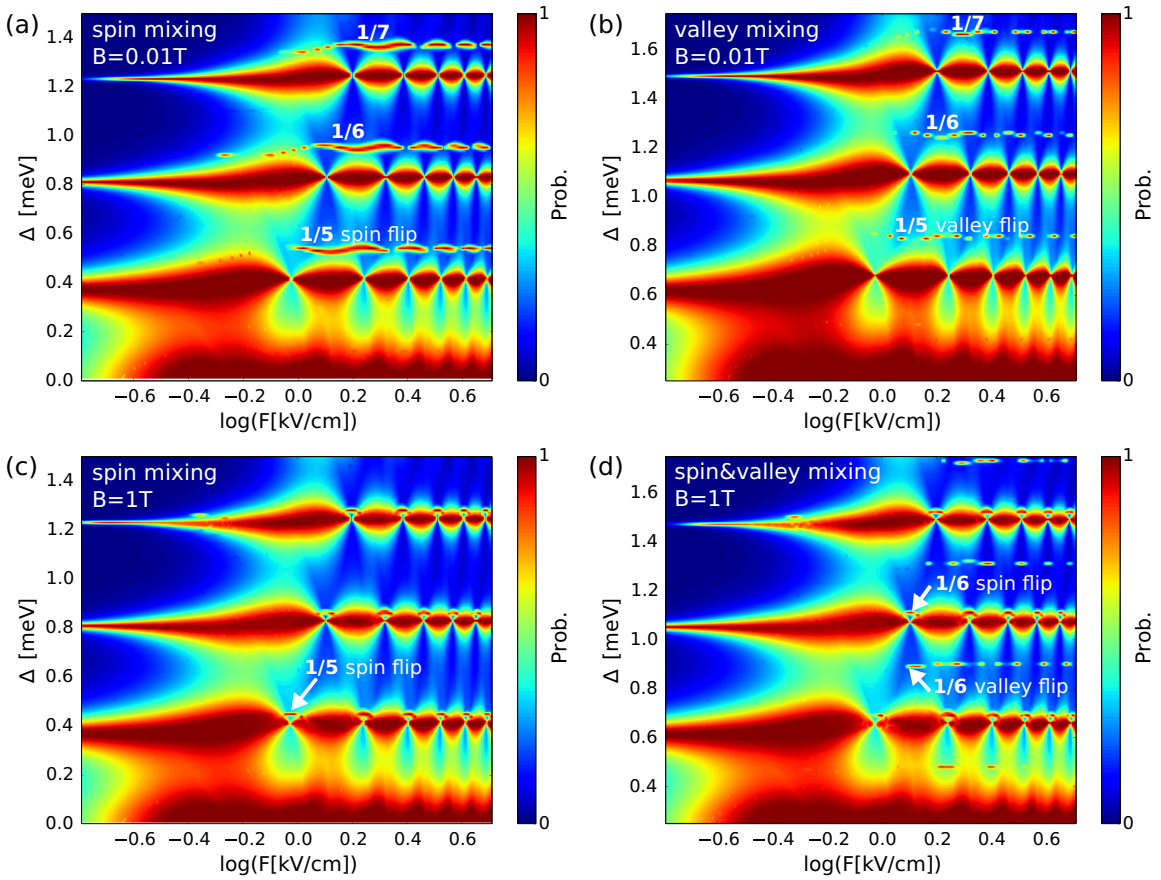

FIG. 5. Maximal probability of the $(1h,0) \rightarrow (0,1h)$ transitions as a function of Δ and a logarithm of the amplitude of the microwave electric field F. We apply an ac electric field of frequency $\hbar\omega = 0.5$ meV within a pulse of duration 1 ns. In panels (a) and (c) the nanotube is assumed bent. In panel (b) the two potential peaks of 1 eV at -14.2 nm and 14.13 nm are introduced in the CNT. In panel (d) both the bending and the potential peaks are considered. In panels (a) and (b) the magnetic field is set close to zero ($B = 0.01$ T); in panels (c) and (d) $B = 1$ T.

lines corresponding to these two transitions are shifted with respect to each other due to the SO splitting of the spin-valley doublets of 2 meV which is constant for every Δ—see Fig. 2(a).

To enable the valley-flipping transitions—i.e., $(1h,0)K' \uparrow \rightarrow (0,1h)K \uparrow$—a short-range potential has to be introduced into the CNT lattice. That type of potential acts as a scattering center which mixes K and K' valleys. In experimental setups the scattering potential might by produced by defects in the lattice. To model the effect in our calculations we introduce two potential peaks of 1 eV at -14.2 and 14.13 nm. This results in additional narrow resonances visible in Fig. 5(b) as opposed to Fig. 3. Similarly to Fig. 5(a), the lines correspond to the one fifth, one sixth, and one seventh of the nominal resonant frequency for the transition $(1h,0)K' \uparrow \rightarrow (0,1h)K \uparrow$. The valley-flipping transitions are shifted with respect to the valley-conserving transitions the same way as transitions of Fig. 5(a). In fact, if both spin and valley mixing are introduced, the resonant lines for spin- and valley-flipping transitions overlap. This can be easily understood by looking at Fig. 2—for $B = 0$ the $(0,1h)K' \downarrow$ and $K \uparrow$ are degenerate.

The position of the resonant lines for spin or valley flipping and spin-valley-conserving transitions with respect to each other depends on the SO energy splitting and the applied ac field frequency. While the SO interaction due to the curvature of the carbon plane is hardly controllable from an experimental point of view, the microwave driving frequency can easily be modulated. For instance, by doubling ω we obtain two times larger gaps between adjacent harmonics on the Δ scale. Another externally tunable parameter which can be used to modify the position of transition lines is the magnetic field B. Distinct behavior of the different spin and valley states in external magnetic field [see Fig. 2(b)] results in changes of the resonant frequencies for spin- and valley-flipping transitions. The spin-valley-conserving transition preserves the same resonant frequency for every B since the energy difference between same spin and valley states of $(1h,0)$ and $(0,1h)$ configurations does not change in magnetic field. In Fig. 5(c) we present spectra for the bent CNT with a magnetic field of $B = 1$ T applied. Here, the narrow spin-flipping resonances of Fig. 5(a) have shifted to lower Δ while spin-valley-conserving transition lines have remained still. As shown in Fig. 5(c), the spin-flipping resonances can be shifted until they overlap with the wider spin-valley-conserving resonances and the two become nearly indistinguishable. The narrow resonances can be observed as a small perturbation in the—otherwise regular—interference pattern of the wide ones.

In Fig. 5(d) we plot the transition spectra for a bent nanotube with the potential peaks introduced in the lattice and magnetic field of $B = 1$ T applied. Here still the

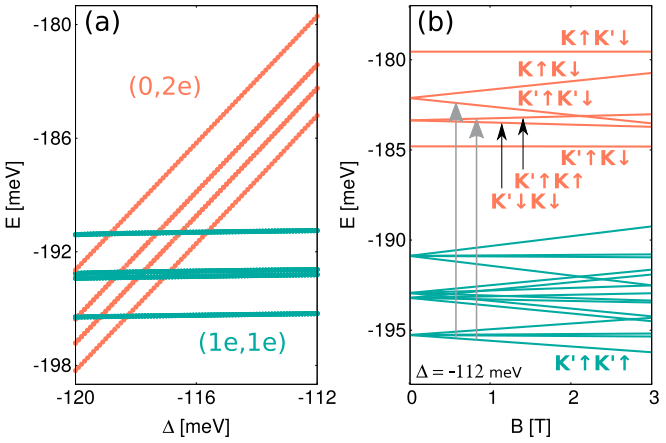

FIG. 6. (a) Two-electron energy levels in *nn* QD as a function of the potential mismatch parameter between the dots Δ. (b) Energy-level dependence on the external magnetic field B for $\Delta = -112$ meV.

spin-valley-conserving and spin-flipping resonances overlap but additional lines of valley-flipping transitions appear, as in Fig. 5(b). Note, however, that these lines are strongly shifted by the magnetic field—for Δ of about 0.9 meV we observe the fifth harmonic for $B \approx 0$ and the sixth harmonic for $B = 1$ T. The valley-flipping transition lines are shifted more than the spin-flipping ones because the energy difference between $(1h,0)K' \uparrow$ and $(0,1h)K \uparrow$ grows faster with B then between $(1h,0)K' \uparrow$ and $(0,1h)K' \downarrow$ [see Fig. 2(b)].

B. $(1e,1e) \rightarrow (0,2e)$ transitions

The two-electron *nn* system provides an entirely different frame for photon-assisted tunneling. The reason is the Pauli blockade, which arises in the ground state of the $(1e,1e)$ charge configuration in the *nn* quantum dot in the external magnetic field [see Fig. 1(c)]. In Fig. 6(a) we present the lowest-energy levels of two-electron *nn* system as a function of Δ and in Fig. 6(b) the effect of the magnetic field B on the energy levels. We are interested in transitions $(1e,1e) \rightarrow (0,2e)$, i.e., tunneling of an electron from the left dot to the right dot. As one can see in Fig. 6(b), in nonzero magnetic field the two electrons in the quantum dots occupy the same spin and valley states (triplet state $K' \uparrow K' \uparrow$), hence the tunneling from one dot to the other is suppressed. In fact, for straight and clean CNTs we do not observe any transitions $(1e,1e)K' \uparrow K' \uparrow \rightarrow (0,2e)$ driven by a microwave electric field. Resonant lines analogous to those in Fig. 3 do not appear in the spectra if the spin-valley blockade persists in the microwave radiation.

However, the blockade can be lifted by mixing the spin or/and valley states which can be achieved—similarly to the *pp* system—by bending the nanotube or introducing defects in the lattice. In Fig. 7(a) we plot the $(1e,1e) \rightarrow (0,2e)$ transition probability for a bent CNT as a function of Δ and a logarithm of the amplitude of the microwave electric field F. We assume the system is initially in the blocked triplet $K' \uparrow K' \uparrow$ state. The only resonances that appear in Fig. 7(a) are very narrow transition lines to the singlet state $(0,2e)K' \uparrow K' \downarrow$.

Figure 7(b) contains the result in presence of the valley-mixing short-range potentials that allow for valley flips along

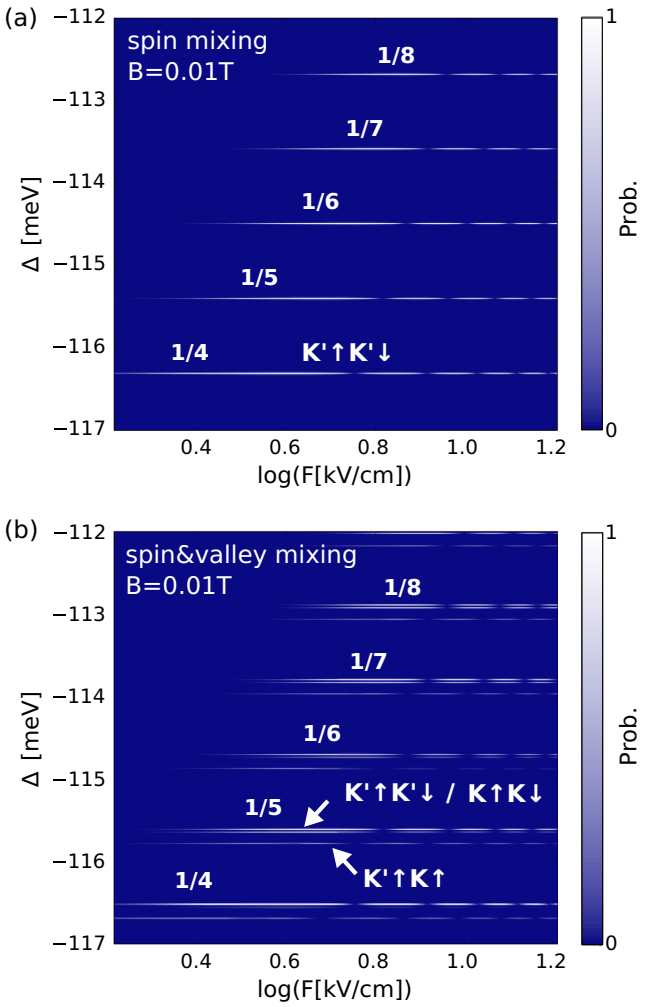

FIG. 7. Maximal probability of the transition $(1e,1e)K' \uparrow K' \uparrow \rightarrow (0,2e)$ for a bent CNT as a function of Δ and a logarithm of the amplitude of the microwave electric field F. In panel (a) the nanotube is assumed bent, in panel (b) the bend and the two potential peaks of 1 eV at -14.2 and 14.13 nm are considered. We apply the electric-field frequency $\hbar\omega = 1.5$ meV within a pulse of duration 1 ns. The final state of the $(0,2e)$ charge configuration is marked in the figure.

the tunneling. Now, the lines split into doublets which correspond to either the spin flip $(1e,1e)K' \uparrow K' \uparrow \rightarrow (0,2e)K' \uparrow K' \downarrow$ or the valley flip $(1e,1e)K' \uparrow K' \uparrow \rightarrow (0,2e)K' \uparrow K \uparrow$. Additionally, the line $(1e,1e)K' \uparrow K' \uparrow \rightarrow (0,2e)K' \uparrow K' \downarrow$ also splits into two, which results from the mixing of the $K' \uparrow K' \downarrow$ and $K \uparrow K \downarrow$ states which is present for weak B. Therefore, two separate spin transition lines are visible in Fig. 7(b) very close on the Δ scale. Other transitions, involving spin and valley transition or the change of both occupied single-electron orbitals, are too weak to be noticed in this plot.

IV. CONCLUSIONS

We have simulated photon-assisted tunneling for a double quantum dot system defined within a carbon nanotube by using the tight-binding approach and the time-dependent configuration-interaction method. We considered unipolar

quantum dots confining either holes or electrons for systems in which the photon-induced charge transition from the ground state to the excited state is either allowed or blocked by the Pauli exclusion principle. For the former case we reproduced the pattern of the LZS interference recently observed [16]. In the latter case in an external magnetic field the ground state of the $(1e,1e)$ charge configuration is a nondegenerate triplet-like spin-valley polarized state [Fig. 6(b)] $K' \uparrow K' \uparrow$ from which the charge transition to $(0e,2e)$ can only occur provided that either the spin or the valley change at the tunneling. The system can be tuned by voltages into a regime where only the ground state is below the Fermi energy of the drain. Then, the photon assisted tunneling can be used to trigger and resolve charge hoppings involving either the spin or the valley transitions.

ACKNOWLEDGMENTS

This work was supported by the National Science Centre according to decision DEC-2013/11/B/ST3/03837. Calculations were performed in the PL-Grid Infrastructure.

[1] L. P. Kouwenhoven, S. Jauhar, J. Orenstein, P. L. McEuen, Y. Nagamune, J. Motohisa, and H. Sakaki, Phys. Rev. Lett. **73**, 3443 (1994).
[2] C. A. Stafford and Ned S. Wingreen, Phys. Rev. Lett. **76**, 1916 (1996).
[3] R. H. Blick, R. J. Haug, K. von Klitzing, and K. Eberl, Surf. Sci. **361-362**, 595 (1996).
[4] T. H. Oosterkamp, T. Fujisawa, W. G. van der Wiel, K. Ishibashi, R. V. Hijman, S. Tarucha, and L. P. Kouwenhoven, Nature (London) **395**, 873 (1998).
[5] C. Meyer, J. M. Elzerman, and L. P. Kouwenhoven, Nano Lett. **7**, 295 (2007).
[6] B.-C. Wang, G. Cao, B.-B. Chen, G.-D. Yu, H.-O. Li, M. Xiao, and G.-P. Guo, J. Appl. Phys. **120**, 064302 (2016).
[7] R. Shang, H. Li, G. Cao, M. Xiao, T. Tu, G.-C. Guo, H.-W. Jiang, and G.-P. Guo, Appl. Phys. Lett. **103**, 162109 (2013).
[8] K. D. Petersson, C. G. Smith, D. Anderson, P. Atkinson, G. A. C. Jones, and D. A. Ritchie, Phys. Rev. Lett. **103**, 016805 (2009).
[9] L. R. Schreiber, F. R. Braakman, T. Meunier, V. Calado, J. Danon, J. M. Taylor, W. Wegscheider, and L. M. K. Vandersypen, Nat. Commun. **2**, 556 (2011).
[10] J. R. Petta, A. C. Johnson, C. M. Marcus, M. P. Hanson, and A. C. Gossard, Phys. Rev. Lett. **93**, 186802 (2004).
[11] T. Kodera, W. G. van der Wiel, K. Ono, S. Sasaki, T. Fujisawa, and S. Tarucha, Phys. E (Amsterdam, Neth.) **22**, 518 (2004).
[12] S. N. Shevchenko, S. Ashhab, and F. Nori, Phys. Rep. **492**, 1 (2010).
[13] J. Stehlik, Y. Dovzhenko, J. R. Petta, J. R. Johansson, F. Nori, H. Lu, and A. C. Gossard, Phys. Rev. B **86**, 121303(R) (2012).
[14] J. R. Petta, H. Lu, and A. C. Gossard, Science **327**, 669 (2010).
[15] L. Gaudreau, G. Granger, A. Kam, G. C. Aers, S. A. Studenikin, P. Zawadzki, M. Pioro-Ladrière, Z. R. Wasilewski, and A. S. Sachrajda, Nat. Phys. **8**, 54 (2012).
[16] A. Mavalankar, T. Pei, E. M. Gauger, J. H. Warner, G. A. D. Briggs, and E. A. Laird, Phys. Rev. B **93**, 235428 (2016).
[17] W. D. Oliver, Y. Yu, J. C. Lee, K. K. Berggren, L. S. Levitov, and T. P. Orlando, Science **310**, 1653 (2005).
[18] M. Sillanpää, T. Lehtinen, A. Paila, Y. Makhlin, and P. Hakonen, Phys. Rev. Lett. **96**, 187002 (2006).
[19] Z. Sun, J. Ma, X. Wang, and F. Nori, Phys. Rev. A **86**, 012107 (2012).
[20] D. Dovinos and D. Williams, Phys. Rev. B **72**, 085313 (2005).
[21] E. Prati, R. Latempa, and M. Fanciulli, Phys. Rev. B **80**, 165331 (2009).
[22] M. F. Gonzalez-Zalba, S. N. Shevchenko, S. Barraud, J. R. Johansson, A. J. Ferguson, F. Nori, and A. C. Betz, Nano Lett. **16**, 1614 (2016).
[23] M. Braun and G. Burkard, Phys. Rev. Lett. **101**, 036802 (2008).
[24] E. A. Laird, F. Kuemmeth, G. A. Steele, K. Grove-Rasmussen, J. Nygård, K. Flensberg, and L. P. Kouwenhoven, Rev. Mod. Phys. **87**, 703 (2015).
[25] T. Ando, J. Phys. Soc. Jpn. **74**, 777 (2005).
[26] D. Huertas-Hernando, F. Guinea, and A. Brataas, Phys. Rev. B **74**, 155426 (2006).
[27] D. V. Bulaev, B. Trauzettel, and D. Loss, Phys. Rev. B **77**, 235301 (2008).
[28] M. del Valle, M. Margańska, and M. Grifoni, Phys. Rev. B **84**, 165427 (2011).
[29] J. Klinovaja, M. J. Schmidt, B. Braunecker, and D. Loss, Phys. Rev. B **84**, 085452 (2011).
[30] K. Flensberg and C. M. Marcus, Phys. Rev. B **81**, 195418 (2010).
[31] E. N. Osika and B. Szafran, J. Phys.: Condens. Matter **27**, 435301 (2015).
[32] E. N. Osika and B. Szafran, Phys. Rev. B **91**, 085312 (2015).
[33] E. N. Osika, A. Mreńca, and B. Szafran, Phys. Rev. B **90**, 125302 (2014).
[34] A. Pályi and G. Burkard, Phys. Rev. Lett. **106**, 086801 (2011).